On the existence of spatially periodic temporally unstable disturbances in two-dimensional convectively unstable Prats flows

# On the existence of spatially-periodic temporally-unstable disturbances in two-dimensional convectively unstable Prats flows

Pedro Vayssière Brandão,[1] Antonio Barletta,[1] Leonardo Santos de Brito Alves,[2] Michele Celli,[1] and Emanuele Ghedini[1]
[1)]*DIN, Alma Mater Studiorum Universita di Bologna, Viale Risorgimento 2, 40136 Bologna, Italy*
[2)]*PGMEC, UFF, Rua Passo da Patria 156, Bloco E, Sala 211, Niteroi, Rio de Janeiro 24210-240, Brazil*

(Dated: 3 July 2024)

In linear and local stability analysis, the small amplitude disturbance behaviour has been well understood for decades. In this context, convectively unstable flows act as noise amplifiers. In other words, a continuous excitation source at a fixed location triggers the spatial growth (or decay) of disturbances downstream of it. Hence, these flows have been traditionally analysed using a spatial stability analysis, where disturbances are assumed temporally-periodic and spatially-unstable. Such a behaviour has been consistently verified by direct numerical simulations. The present investigation shows that this agreement indeed occurs, but only close enough to the excitation source under certain parametric conditions. When the excitation source triggers disturbances that decay in space, far away from this source, spatially-periodic and temporally-unstable disturbances are allowed to grow and become dominant. Evidence for the scenario just described is provided using direct numerical simulations of the two-dimensional Prats problem.

## I. INTRODUCTION

The distinction between convective and absolute instabilities lies in the long-time behaviour of an infinitesimal wavepacket introduced in a fixed spatial location. If the wavepacket amplitude decays in this limit, at its excitation point, the flow is stable or convectively unstable. Otherwise, the flow is absolutely unstable. A good definition and review of this concept can be found in the paper by Huerre and Monkewitz [1], as well as in the books by Drazin and Reid [2] and Barletta [3].

In a convectively unstable regime, disturbances grow in amplitude as they are convected away from their excitation source. When this source acts over a finite period of time, they eventually leave the domain, returning the flow to its equilibrium state. On the other hand, when this excitation source emits a continuous time periodic signal at an unstable frequency, disturbances that oscillate at this same frequency and grow in time are continuously generated and convected downstream. In this case, an observer should see, in an asymptotic regime, disturbances that are temporally-periodic and spatially-unstable (grow in space at given instant of time). Instead, if the excitation source emits a continuous time periodic signal at a stable frequency, disturbances that oscillate at this same frequency are damped in time. In this situation, the observer sees disturbances that are temporally-periodic and spatially-stable (decay in space at given instant of time).

The pioneering stability analyses that identified the parametric condition characterizing the onset of convective instabilities in a fluid saturated porous medium were reported by Horton and Rogers Jr [4] and by Lapwood [5]. Later on, Prats [6] investigated the effect of a basic throughflow on this onset. In the following years, several analyses have been done by considering additional effects, such as different ways of heating or different kinds of fluids [7–10]. The analyses mentioned above are related to the study of spatially-periodic disturbances that can grow in time. When a zero temporal growth rate is imposed, the onset of convective instability can be determined for these cases.

Another way to understand instability is to consider temporally-periodic disturbances that can grow in space. This approach is usually employed in a spatial stability analysis to investigate the flow behaviour when it is convectively unstable. There are not many studies in the literature dealing with spatial stability analyses, especially in the context of fluid saturated porous media. Delache, Ouarzazi, and Combarnous [11] investigated the spatio-temporal instability of mixed convective flows

in porous media, without detailing all the features relative to the spatial framework, focusing on the transition to absolute instability. Results for the transition to absolute instability of this problem can be also find in Barletta and Alves [12] and Barletta [3].

Spatially unstable problems can be treated as initial values problems[13–15]. The idea, in that case, is to consider the forcing oscillator as acting only for $t > 0$. In this sense, due to the persistence of the initial condition, the spatial instability branches are divided into those that exist downstream and upstream of the source. This problem, also known as the signaling problem, was first analysed by Gaster [16]. Recently, Barletta [17,18] investigated the spatially developing modes on the Prats problem by means of the linear theory. Barletta considered temporally-periodic disturbances that have no memory of the initial conditions. For this reason, the persistence of the initial conditions is not an issue here. As expected, instead of the single mode found in a temporal stability analysis, this author found four modes. These particular spatial stability results, however, provide a perspective different from that of an initial value problem.

Nonlinear simulations are often used both to validate and to give further insights into the theoretical results. Dufour and Neel [19] have investigated this same problem by means of numerical simulation, without detailing the spatial behaviour of disturbances developing from a source. They focused on self-sustained oscillations, which appear above the absolute instability threshold. Then, Dufour and Néel [20] demonstrated the existence of the time-periodic convective patterns between the convective and the absolute instability thresholds. It is important to note that they did not find spatially-periodic disturbances in this convectively unstable flow.

The present paper, on the other hand, identifies conditions where the disturbance behaviour does not necessarily follow the trends of the studies mentioned before. This is observed in direct numerical simulations of the Prats problem. In the present study, we remain always below the absolute instability threshold in order to avoid the possibility of self-sustained oscillations. In addition, we remain above the convective instability threshold.

The goal is to investigate the existence of spatially-periodic temporally-unstable disturbances in the Prats flow excited by a time periodic source located at a fixed spatial position. In other words, we aim to demonstrate that, in a convectively unstable regime, even when temporally-periodic spatially-stable disturbances are excited, spatially-periodic temporally-unstable disturbances may appear far enough from the excitation source.

A buffer zone is employed at the outlet to avoid numerical waves propagating back into the solution, in order to emulate a semi-infinite domain. Hence, the present study cannot be classified as being part of either temporal or spatial instability studies in the sense described above. It is set up in such a way as to allow both types of modes to co-exist. The next section presents the Prats problem to the reader, the following two sections describe in detail the mathematical formulation of this problem and the numerical tools employed to solve it, respectively. They are followed by a results section, showing the co-existence of both disturbances types. The paper then ends with conclusions and future work. An appendix is also included to summarize the extensive parametric numerical study performed to make sure that the observed behaviour is physical and not a numerical artefact.

## II. PRATS PROBLEM

The appearance of convective cells in an initially purely conductive state is an important phenomenon that is nowadays widely explored in the literature. Studies in this area started with the experiments carried on by Bénard [21], in which he observed the appearance of convective cells in a layer of fluid heated from below. Such convective cells could be observed just for certain values of the temperature difference between the upper and lower bounds. In other words, there is a critical temperature difference beyond which there succeed a transition between these two different regimes. Later on, Lord Rayleigh [22] proposed the first theoretical explanation for this phenomenon, by considering buoyancy as the driving mechanism of it. Based on small disturbances analysis, he was able to find a theoretical value for such critical temperature difference. In honour of these two important pioneering contributions, the phenomenon of buoyancy-driven convection in a fluid layer is known nowadays as Rayleigh-Bénard (RB) convection.

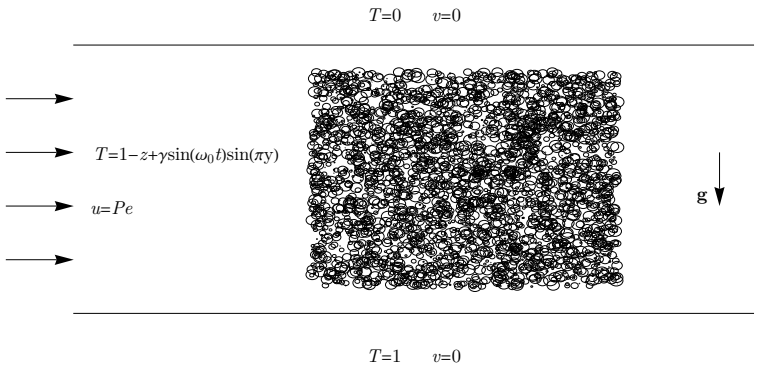


FIG. 1. Sketch of the problem.

The counterpart of the RB problem for a porous media is also known as Horton-Rogers-Lapwood (HRL) problem, in honour of the pioneering works made by Horton and Rogers Jr[4] and by Lapwood[5] in this field. They investigated the appearance of convective cells in a porous medium saturated by a Newtonian fluid at rest bounded by horizontal impermeable walls at prescribed temperatures. In order to the convective cells to take place, the lower wall must be hotter than the upper one. They found that the critical dimensionless temperature difference (which is given by the Darcy-Rayleigh number) for this case is $R = 4\pi^2$.

As mentioned in the last Section, Prats[6] was responsible to take into consideration the effect of a throughflow in the analysis of the HRL problem. He found that the presence of the throughflow did not affect the critical temperature difference, but only the characteristics of the convective motion. Namely, in the presence of throughflow the emerged convective cells are not stationary, but oscillatory. For this reason, the problem of investigating the emergence of convective cells in a saturated porous medium with uniform throughflow is nowadays called Prats problem. Theoretical and experimental investigations have found that the convective structures emerging in the transition to instability in the Prats problem are transverse, and consequently two-dimensional[9,23].

## III. MATHEMATICAL FORMULATION

A two-dimensional fluid saturated porous layer of height $H$, represented in Figure 1, is considered. The flow is defined in the $(x,y)$ plane, where the $y$ axis is vertical. The fluid is assumed to be Newtonian and the layer is horizontal and bounded by impermeable $y = constant$ walls with prescribed temperatures. The lower wall at $y = 0$ has a temperature $T = T_h$, while the upper wall at $y = H$ has a temperature $T = T_c < T_h$. In the basic stationary state, the fluid is assumed to flow with a constant Darcy velocity $u_0$ and the layer is assumed to be infinitely wide in the flow direction. Local thermal equilibrium between the fluid and solid phases is invoked. The Oberbeck-Boussinesq approximation is adopted where the momentum balance equation is given by Darcy's law. The mass balance, momentum balance and energy balance equations are represented in the following dimensionless formulation:

$$\nabla \cdot \boldsymbol{u} = 0, \tag{1}$$

$$\boldsymbol{u} = -\nabla P - RT\boldsymbol{g}, \tag{2}$$

$$\frac{\partial T}{\partial t} + \boldsymbol{u}\cdot\boldsymbol{\nabla} T = \nabla^2 T, \tag{3}$$

with the boundary conditions

$$y = 0: \quad v = 0,\ T = 1, \tag{4a}$$

$$y = 1: \quad v = 0,\ T = 0. \tag{4b}$$

The scaling adopted to nondimensionalize Eqs. (1)-(4) is defined as

$$\boldsymbol{u}\frac{H}{\alpha} \to \boldsymbol{u}, \quad \boldsymbol{x}\frac{1}{H} \to \boldsymbol{x}, \quad t\frac{\alpha}{\sigma H^2} \to t, \quad \frac{T - T_c}{T_h - T_c} \to T, \quad P\frac{K}{\alpha\mu} \to P. \tag{5}$$

Here, $\boldsymbol{u} = (u, v)$ is the velocity vector, $\alpha$ is the effective thermal diffusivity, $\boldsymbol{x} = (x, y)$ is the Cartesian coordinate vector, $\sigma$ is the heat capacity ratio, $P$ is the difference between the pressure and the hydrostatic pressure, $K$ is the permeability of the medium, $\mu$ is the dynamic viscosity and $\boldsymbol{e}_y$ is the unit vector in the vertical direction. The gravitational acceleration is $\boldsymbol{g} = -g\boldsymbol{e}_y$, where $g$ denotes the modulus of $\boldsymbol{g}$. Two dimensionless groups emerge from this procedure,

$$R = \frac{\rho g \beta (T_h - T_c) H K}{\mu \alpha}, \quad \text{and} \quad Pe = \frac{u_0 H}{\alpha}, \tag{6}$$

namely, the Darcy-Rayleigh number and the Péclet number, respectively. In Eq. (6), $\rho$ is the fluid density at the reference temperature, which is chosen to be $T_c$, and $\beta$ is the thermal expansion coefficient.

### A. Stationary solution

As already mentioned, the objective here is understanding how infinitesimal disturbances develop, in time and space, from a source placed at a given position. More specifically, the task is understanding how an equilibrium solution responds to infinitesimal disturbances generated by a periodic source localized in space. This is done by considering simulations of large enough domains over long enough times to allow for the existence of both temporally and spatially-periodic disturbances. In order to do so, it is necessary to define a steady-state.

The stationary solution of Eqs. (1)-(4) is the conductive state for the temperature field induced by the temperature difference between the vertical walls

$$\overline{T}(y) = 1 - y, \tag{7}$$

where the overline is hereafter employed to denote the quantities relative to the stationary solution. The dimensional throughflow velocity in the longitudinal direction is $u_0$ which, in a dimensionless formulation, becomes $Pe$. In a conductive regime, no flow is expected to take place in the vertical direction. Hence, the stationary solution of Eqs. (1)-(4) for the velocity field is given by

$$\overline{\boldsymbol{u}} = (Pe, 0). \tag{8}$$

### B. Streamfunction-temperature formulation

In order to solve numerically Eqs. (1)-(4), some efforts can be made to simplify the numerical treatment without losing any generality in the physics. As mentioned before, according to theoretical and experimental results, the convective patterns that first emerge in the vicinity of the convective instability threshold in the Prats problem are transverse, and consequently two-dimensional[23].

This fact allow us to treat the problem by means of a two-dimensional streamfunction-temperature formulation of the balance equations, namely

$$\nabla^2\psi = -R\frac{\partial T}{\partial x}, \tag{9}$$

$$\frac{\partial T}{\partial t} + \frac{\partial \psi}{\partial y}\frac{\partial T}{\partial x} - \frac{\partial \psi}{\partial x}\frac{\partial T}{\partial y} = \nabla^2 T. \tag{10}$$

The boundary conditions, for the present formulation, are rewritten as

$$y = 0: \quad \frac{\partial \psi}{\partial x} = 0, T = 1, \tag{11a}$$

$$y = 1: \quad \frac{\partial \psi}{\partial x} = 0, T = 0, \tag{11b}$$

with

$$u = \frac{\partial \psi}{\partial y}, \quad v = -\frac{\partial \psi}{\partial x}. \tag{12}$$

The stationary solution for the streamfunction variable, considering the definition (12) and the stationary solution for the velocity (8), is given by

$$\overline{\psi} = Pe\, y + constant, \tag{13}$$

where the constant is defined in such a way to have $\overline{\psi}(y = 0) = 0$.

## IV. NUMERICAL PROCEDURE

The direct numerical simulation is performed here by means of finite-difference-based methods. The discretization of the convective terms in the energy equation (10) uses the third-order upwind scheme, while the diffusive terms are discretized by the fourth-order central finite difference scheme. The time integration is done by the third-order Runge-Kutta scheme. The Poisson's equation (9) is solved by means of an over-relaxed Gauss-Seidel method. The relaxation parameter is assumed to be equal to 1.9. More details about the simulations that generated the results shown in the following section are discussed next. However, it must be emphasized here that several other tests were performed to make sure these results are physical and not numerical artefacts. These additional tests are briefly described in Appendix A.

### A. Initial, inlet and outlet conditions

The problem is initially formulated for a semi-infinite domain in the longitudinal direction. For obvious reasons, it is not possible to simulate numerically a truly semi-infinite domain. Therefore, it is imperative to truncate the domain.

The initial condition is considered to be the same stationary solution presented in the previous section. By assuming that the fluid is moving in the positive direction of the longitudinal axis $x$, inlet and outlet boundary conditions for this direction are considered. The inlet condition is defined by equation (15). At the outlet, it is assumed a zero normal derivative boundary condition for both streamfunction and temperature, namely

$$\left.\frac{\partial T}{\partial x}\right|_{x=L} = 0, \quad \left.\frac{\partial \psi}{\partial x}\right|_{x=L} = 0. \tag{14}$$

In order to investigate the flow response to infinitesimal disturbances, we localize the periodic source at the inlet, i.e. $x = 0$. In other words, the inlet condition is formed by a superposition of the stationary solution and a temporal oscillator in the form of,

$$T(x = 0, y, t) = \overline{T}(y) + \gamma \sin(\omega_o t) \sin(\pi y), \tag{15}$$

where $\omega_o$ is the oscillation frequency, $\gamma$ is the amplitude coefficient, and the $y$-dependence is chosen in such a way as to satisfy the boundary conditions at the upper and lower walls. Here, we assume $\gamma = 10^{-3}$.

### B. Non-reflecting boundary condition

As disturbances start to grow, and the solution departs from the stationary regime, numerical reflection issues might arise when these disturbances reach the outlet of the domain. Here, we adopted a technique, developed for aerodynamic and aeroacoustic simulations, that attempts to impose a non-reflecting boundary condition to avoid such problems. This technique consists of introducing a buffer in a specific area of the computational domain within which the solution is smoothly attenuated and forced to converge to a desirable target, without producing a reflection. Further details about this technique can be found in Freund [24] and Richards *et al.* [25].

There are three distinct ways of applying this technique: (i) explicitly, after each time step; (ii) implicitly, by adding the buffer in the governing equations; (iii) implicitly, by adding an artificial convection in the governing equations. In the present work, only (i) and (ii) are considered. The second type is applied in the energy equation, in order to damp temperature, while the first type is applied directly to the streamfunction variable after each solution of Poisson's equation.

The first type can be represented by

$$\hat{\psi} = \psi - \delta(x) \left(\psi - \psi_{\text{target}}\right), \tag{16}$$

where $\hat{\psi}$ is the damped streamfunction, $\delta$ is the damping function and $\psi_{\text{target}}$ is the reference solution towards which the solution is forced to converge in the buffer zone. For the second type, the buffer is added to the energy equation

$$\frac{\partial T}{\partial t} + \frac{\partial \psi}{\partial y}\frac{\partial T}{\partial x} - \frac{\partial \psi}{\partial x}\frac{\partial T}{\partial y} = \nabla^2 T - \delta(x) \left(T - T_{\text{target}}\right), \tag{17}$$

where, analogously, $T_{\text{target}}$ is the reference solution to which the solution is forced to converge in the buffer zone. The damping function $\delta(x)$ is defined by

$$\delta(x) = \begin{cases} 0 & 0 \le x \le L - l \\ \delta_m \left[\frac{x-(L-l)}{l}\right]^b & L - l \le x \le L, \end{cases} \tag{18}$$

where $l$ represents the dimension of the buffer zone at the outlet and $\beta$ represents the form of the damping curve. Here, $l = 3$, $\delta_m = 10^4$, $b = 2$ and $L = 100$. In this study, the stationary solution is used as the reference solution.

| $\Delta x = \Delta y$ | wavenumber | spatial growth-rate |
|---|---|---|
| 1/10 | 2.89272 | 0.466697 |
| 1/15 | 2.87805 | 0.467054 |
| 1/20 | 2.87425 | 0.468653 |
| 1/25 | 2.87149 | 0.468616 |
| 1/30 | 2.87090 | 0.469331 |
| LSA | 2.84295 | 0.515850 |

TABLE I. Wavenumber and spatial growth-rate obtained by interpolating the streamfunction disturbance for $R = 50$, $Pe = 10$ and $\omega_o = 30$; dimensionless time $t = 10$ and time step $\Delta t = 10^{-5}$; results from linear stability analysis (LSA) are presented in the bottom line.

## V. DISCUSSION OF THE RESULTS

Results are presented for the streamfunction perturbation field, which is obtained by subtracting the steady state from the total field. All simulations have been done with a fixed time step of $\Delta t = 10^{-4}$ and a fixed spatial resolution of $\Delta x = \Delta y = 1/25$. Mesh and time step convergence studies were performed for the particular case of $R = 50, Pe = 10$ and $\omega_o = 30$ using the disturbance wavenumber and spatial growth-rate measured just downstream of the source. Higher $Pe$ flow simulations require higher temporal and spatial resolutions. This is the reason why the temporal and spatial resolutions specified for the higher $Pe$ chosen for the verification study is maintained when studying the physics behind the smaller $Pe$ cases discussed. Tables I and II show these results for a fixed temporal resolution and a fixed spatial resolution, respectively, at dimensionless time $t = 10$. This results are the aim of doing a convergence analysis of the spatio-temporal resolution of the numerical procedure. While the results for wavenumber coincide well with those from the linear analysis, there is a higher discrepancy for the results concerning the spatial growth-rate. It is expected that linear stability results can be reproduced in asymptotic regimes. In order to get more accurate results for the spatial growth-rates, larger values of the dimensionless time should be considered. Even so, a reasonable agreement between ours and linear results can be found for both wavenumber and spatial growth-rate. These results justify the aforementioned resolution choices.

In order to understand the transition process, the streamfunction disturbance spatial spectra at different times and temporal spectra at different positions are analysed. Since we are interested in the dominant modes, i.e. their wavenumber and frequency, each spectrum presented here has been normalized to its maximum. In order to compute the spatial and temporal spectra for this problem, we consider the discrete Fourier transform of the streamfunction disturbances

$$\Psi_p = \sum_{q=1}^{N} (\psi - \overline{\psi})_q \exp^{\frac{i2\pi(q-1)(p-1)}{N}}, \tag{19}$$

where $\Psi$ represents the discrete Fourier transformed variable, $\psi - \overline{\psi}$ is the disturbance streamfunction, $q$ is the primitive discrete independent variable, $p$ is the transformed discrete independent variable and $N$ is the number of points of the discrete domain (temporal or spatial). It is important to note that the general form of this transformation is the same one for both spatial and temporal transformations. In the spatial case, $p$ is related to the wavenumber, while in the temporal case $p$ is related to the frequency.

For the next results, we considered two values of $Pe$, namely $Pe = 2$ and $Pe = 5$. Since we are interested in convectively unstable regimes, we consider values of control parameters that are within this range. The onset of convective instability occurs, for every $Pe$, at $R = 4\pi^2 \simeq 39.4784$. The transition to absolute instability, it occurs at $R = 40.4548$ for $Pe = 2$ and at $R = 45.0276$ for $Pe = 5$[7,9]. For this reason, we set $R = 40$ for $Pe = 2$ and $R = 43$ for $Pe = 5$ in the following analysis.

| $\Delta t$ | wavenumber | spatial growth-rate |
|---|---|---|
| $1\times10^{-4}$ | 2.86787 | 0.469472 |
| $5\times10^{-5}$ | 2.86970 | 0.469167 |
| $1\times10^{-5}$ | 2.87149 | 0.468616 |
| LSA | 2.84295 | 0.515850 |

TABLE II. Wavenumber and spatial growth-rate obtained by interpolating the streamfunction disturbance for $R=50$, $Pe=10$ and $\omega_o=30$; dimensionless time $t=10$ and spatial resolution $\Delta x=\Delta y=1/25$; results from linear stability analysis (LSA) are presented in the bottom line.

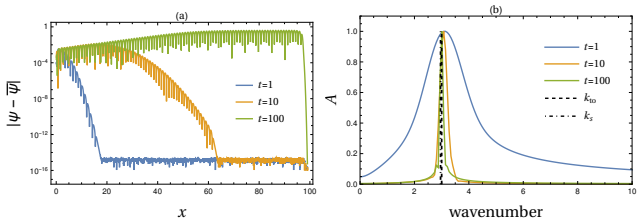


FIG. 2. Streamfunction disturbance distribution (a) for $Pe=2$, $R=40$ and $\omega_o=6$ for different instants of time and its respective spatial spectrum (b); dashed line represent the wavenumber $k_{to}=3$ obtained from temporal analysis at $Pe=2$, $R=40$ and $\omega_o=6$; dot-dashed line represent the wavenumber $k_s=2.95949$ obtained from spatial analysis at $Pe=2$, $R=40$ and $\omega_o=6$.

Figures 2 (a) to 5 (a) show the absolute value of the streamfunction disturbance distribution along $x$ for the fixed value of $y=0.5$ and (b) their respective spatial spectra, where $A$ is the normalized amplitude of $\Psi_p$. Figures 2 (a) and 4 (a) suggest a spatial amplification of the disturbances from the inlet. On the other hand, Figures 3 (a) and 5 (a) show an initial spatial decay from the periodic source followed by a growth at large times.

Figures 2 (b) and 4 (b) show that, for $t=100$, the dominant modes remain quite close to the wavenumber $k_{to}=3$ (dashed line), which is obtained from the temporal analysis considering the source oscillation frequency $\omega_o$. In this case, it is possible to demonstrate that the angular frequency is given by $\omega=kPe$. In fact, $k_{to}=\omega_o/Pe=3$, which is close to $k_s$ for both cases. The wavenumber $k_s$, relative to the spatial instability mode that should be observed in a initial value problem according to the signalling theory[13–15] is represented by the dot-dashed line. The spectra peaks seem to be closer to $k_{to}$, even if $k_s$ is also very close to these values.

On the other hand, Figures 3 (b) and 5 (b) show that, for long times, the dominant mode wavenum-

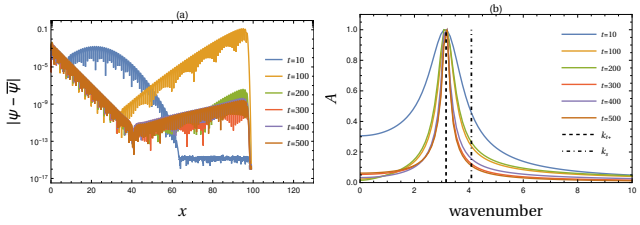


FIG. 3. Streamfunction disturbance distribution (a) for $Pe=2$, $R=40$ and $\omega_o=10$ for different instants of time and its respective spatial spectrum (b); dashed line represent the wavenumber $k_{t+}=3.16222$ relative to the disturbance with maximum growth rate obtained from temporal analysis at $Pe=2$ and $R=40$; dot-dashed line represent the wavenumber $k_s=4.09292$ obtained from spatial analysis at $Pe=2$,$R=40$ and $\omega_o=10$.

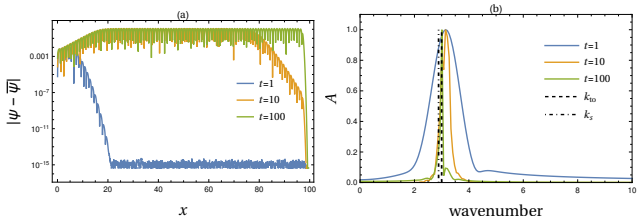


FIG. 4. Streamfunction disturbance distribution (a) for $Pe = 5$, $R = 43$ and $\omega_o = 15$ for different instants of time and its respective spatial spectrum (b); dashed line represent the wavenumber $k_{to} = 3$ obtained from temporal analysis at $Pe = 5$, $R = 43$ and $\omega_o = 15$; dot-dashed line represent the wavenumber $k_s = 2.88725$ obtained from spatial analysis at $Pe = 5$, $R = 43$ and $\omega_o = 15$.

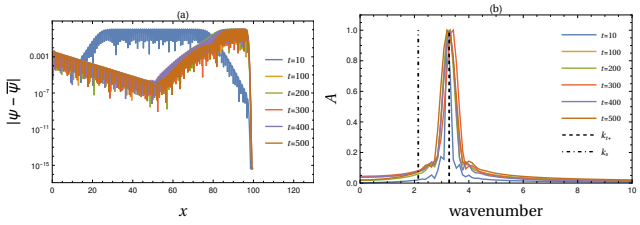


FIG. 5. Streamfunction disturbance distribution (a) for $Pe = 5$, $R = 43$ and $\omega_o = 10$ for different instants of time and its respective spatial spectrum (b); dashed line represent the wavenumber $k_{t+} = 3.27596$ relative to the disturbance with maximum growth rate obtained from temporal analysis at $Pe = 5$ and $R = 43$; dot-dashed line represent the wavenumber $k_s = 2.13929$ obtained from spatial analysis at $Pe = 5$, $R = 43$ and $\omega_o = 10$.

ber is almost equal to $k_{t+}$, which is the wavenumber, computed from temporal analysis, relative to the maximum temporal growth rate. If the source excites an unstable spatial mode, one expects their frequencies to match. Figures 6 and 7 show the temporal spectra of the disturbances measured at $y = 0.5$ and different positions along $x$. For the cases in which the source frequency excites directly an unstable temporal mode (a), the dominant frequency observed is the oscillator frequency $\omega_o$ (dot-dashed line). Instead, for the cases in which the unstable temporal modes are not excited directly by the source (b), the dominant frequency is $\omega_o$ only in the vicinity of the source. Far from it, the dominant frequency is that predicted by the temporal analysis with largest temporal growth rates, $\omega_{t+}$ (dashed line).

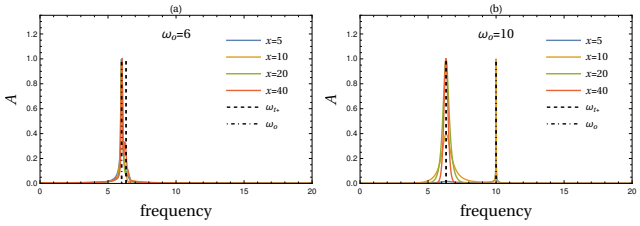


FIG. 6. Temporal spectra of streamfunction disturbance for $Pe = 2$, $R = 40$, $\omega_o = 6$ (a) and $\omega_o = 10$ (b) for different positions in the spatial domain; $\omega_{t+} = 6.32444$.

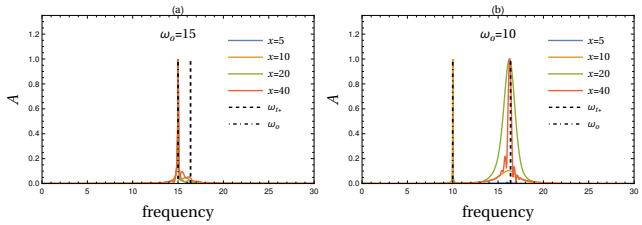


FIG. 7. Temporal spectra of streamfunction disturbance for $Pe = 5$, $R = 43$, $\omega_o = 15$ (a) and $\omega_o = 10$ (b) for different positions in the spatial domain; $\omega_{t+} = 16.3793$.

These results suggest that, when the oscillator frequency does not excite directly an unstable temporal mode, the solution is dominated by the temporal mode with the largest growth rate. In fact, the dominant modes in Figures 3 (b) and 5 (b) seem to coincide with those relative to the must unstable mode $k_{t+} = 3.16$ and $k_{t+} = 3.27$, respectively. In the same way, the dominant frequencies far from the source in Figures 6 (b) and 7 (b), coincide with the frequency of the most unstable modes, $\omega_{t+} = 6.32444$ and $\omega_{t+} = 16.3793$, respectively. Furthermore, the temporal spectra for $x = 5$ indicate that, near the source, the frequency is always coincident to that of the source. This evidence indicates that, in the vicinity of the oscillator, the spatial modes can be present and dominant. Away from the source, the dynamics seems to be entirely determined by the dominant temporal mode. It is important to remark that, in Figures 6 (a) and 7 (a), the temporal spectra is calculated for dimensionless time up to $t = 100$, while for Figures 6 (b) and 7 (b) it is done up to $t = 500$. This is done here in order to avoid the presence of harmonic modes due to the nonlinear saturation.

The linear stability results used here to facilitate the comprehension of the nonlinear results were obtained from the analytical dispersion relation presented by Barletta [18]. This relation is the same for both temporal and spatial analyses. In practice, the only difference is that the frequency is real and the wavenumber is complex for a spatial analysis, while the wavenumber is real and the frequency is complex for a temporal analysis. The analytical expression for the dispersion relation is given by[18]

$$-k^2 - \pi^2 + i\omega + \frac{k^2 R}{k^2+\pi^2} - ikP = 0, \tag{20}$$

where $k$ is the wavenumber and $\omega$ is the frequency. In a temporal approach, by fixing a real value for $k$ it is possible to obtain the complex value of $\omega$ for each assigned value of $P$ and $R$. On the other hand, in a spatial approach, it is possible to obtain the complex value of $k$ by fixing a real value of $\omega$. Figure 8 shows how the frequency varies as a function of the real wavenumber for both temporal (continuous curves) and spatial (dashed curves) analyses. Basically, if one expect the disturbance behaviour to follow the spatial linear analysis, it is sufficient to look for the correspondent wavenumber ($k_s$) relative to $\omega_o$ in Figure 8 (b) and its correspondent growth rate given by Figure 8 (a). On the other hand, the most unstable temporal modes are given by the correspondent wavenumber ($k_{t+}$) of the maximum value of the continuous curves in Figure 8 (a), with $\omega_{t+}$ being the correspondent frequency of such wavenumber.

## VI. CONCLUSIONS

In the present study, we provided evidence for the existence of spatially-periodic temporally-unstable disturbances in the convectively unstable Prats flow. We considered a source located at $x = 0$ that produced a time-periodic signal with a constant frequency. The nonlinear equations were solved directly by means of a high-order finite difference scheme. The main results can be summarized as follows:

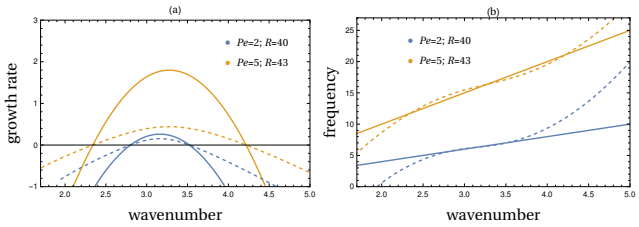


FIG. 8. Temporal (solid curves) and spatial (dashed curves) growth rate (a) and oscillation frequency (b) versus wavenumber computed from linear stability analysis[18].

1. Near the excitation source, temporally-periodic spatially-stable/unstable modes emerge and decay/grow downstream with the same frequency.

2. When the temporally-periodic mode excited is spatially-unstable, spatially-periodic temporally-unstable modes do not appear. Otherwise, spatially-periodic temporally-unstable modes eventually appear far from the excitation source.

3. When the excitation source frequency is within the range of temporally-unstable frequencies of the spatially-periodic mode, they will have the same frequency. Otherwise, the spatially-periodic mode with the highest temporal growth rate appears.

4. Nonlinear simulations were performed under several different numerical conditions (see Appendix A), but they all yield similar results, strongly suggesting that these results are physical and not numerical artefacts.

Although the present results are specific for the two-dimensional Prats problem, we have no reason to think that this dynamics should change for three-dimensional problems. For this reason, we believe that this same dynamics could be observed for other types of parallel flows.

The present results suggest several new research paths. For instance, one could investigate if the same trends observed here are indeed observed in other convectively unstable flows. This can be done for instabilities that are either thermal or hydrodynamic in nature. Examples of the former include the Prats problem in the presence of viscous dissipation, as well as the effect of local thermal non-equilibrium and anysotropic media. Examples of the latter include Poiseuille and Couette flows. A specially important and challenging development, is an alternative nonlinear approach where the focus is on the time-periodic regime induced by the oscillating source of the flow disturbances. Such different paths will be the subject of future investigation.

## ACKNOWLEDGMENTS

This research has been partially funded by the Horizon Europe CoBRAIN (GA No. 101092211).

### Appendix A: Numerical tests

In order to guarantee that the results shown here are physically meaningful, and not a byproduct of undesirable numerical influences, the following parametric tests were performed:

1. Different values for the disturbance amplitude ($\gamma$ in equation (15)) in $x = 0$: $\gamma = 10^{-3}, 10^{-5}, 10^{-7}$.

2. Different lengths for the horizontal channel: $L = 20, 50, 100, 150, 200$.

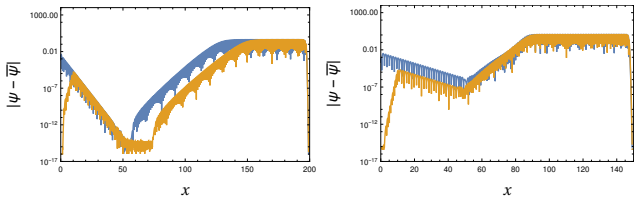


FIG. 9. Comparison between different locations of the excitation source for $Pe = 2$, $\omega = 10$, and $R = 40$ (left) and $Pe = 5$, $\omega = 10$, and $R = 43$ (right).

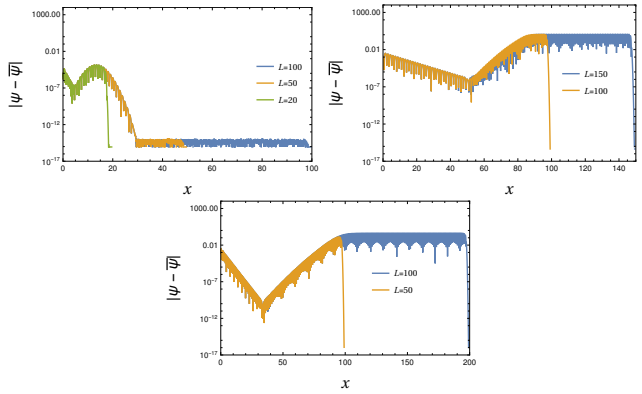


FIG. 10. Comparison between different dimensions of the channel for $Pe = 10$, $\omega = 80$, and $R = 45$ (top-left), $Pe = 5$, $\omega = 10$, and $R = 43$ (top-right) and $Pe = 2$, $\omega = 10$, and $R = 40$ (bottom).

3. Different locations for the excitation source: inlet, outlet, and middle of the domain. At the inlet and outlet boundaries, the disturbances are introduced in the same way, as described by equation (15). On the other hand, when introducing the disturbances in the middle of the domain, a Gaussian-like source term was added to the energy equation. Introducing the disturbances at the outlet provides different results from a physical perspective. Since we are below the absolute instability threshold, there should be no disturbance waves travelling upstream, in such a way that in this case the disturbances travel directly outside the domain, leaving the domain undisturbed.

4. Different buffer parameters. From these tests, the optimal parameters defined in Section IV B were determined.

All the tests mentioned above provided the same behaviour of the numerical results, as it can be confirmed by Figures 9-12. For each figure, the same simulation time was considered for the different cases. This fact leads us to believe that the numerical scheme is robust and the results observed are indeed physically meaningful.

[1]P. Huerre and P. A. Monkewitz, "Local and global instabilities in spatially developing flows," Annual Review of Fluid Mechanics **22**, 473–537 (1990).
[2]P. G. Drazin and W. H. Reid, *Hydrodynamic Stability* (Cambridge University Press, 2004).
[3]A. Barletta, *Routes to Absolute Instability in Porous Media* (Springer, 2019).
[4]C. W. Horton and F. T. Rogers Jr, "Convection currents in a porous medium," Journal of Applied Physics **16**, 367–370 (1945).

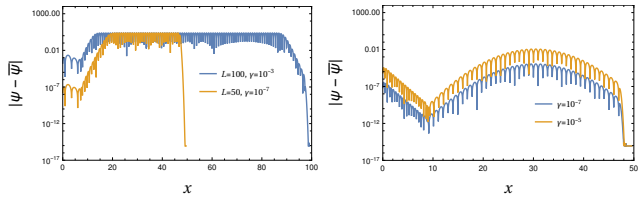


FIG. 11. Comparison between different disturbances magnitudes for $Pe = 10$, $\omega = 10$, and $R = 55$ (left) and $Pe = 10$, $\omega = 80$, and $R = 45$ (right).

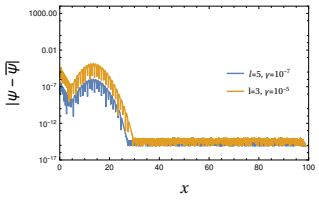


FIG. 12. Comparison between different dimensions of the buffer zone for $Pe = 10$, $\omega = 80$ and $R = 45$

[5]E. R. Lapwood, "Convection of a fluid in a porous medium," Mathematical Proceedings of the Cambridge Philosophical Society **44**, 508–521 (1948).
[6]M. Prats, "The effect of horizontal fluid flow on thermally induced convection currents in porous mediums," Journal of Geophysical Research **71**, 4835–4838 (1966).
[7]S. C. Hirata and M. N. Ouarzazi, "Three-dimensional absolute and convective instabilities in mixed convection of a viscoelastic fluid through a porous medium," Physics letters A **374**, 2661–2666 (2010).
[8]P. Brandão, A. Barletta, M. Celli, L. d. B. Alves, and D. Rees, "On the stability of the isoflux Darcy–Bénard problem with a generalised basic state," International Journal of Heat and Mass Transfer **177**, 121538 (2021).
[9]P. Brandão, L. d. B. Alves, D. Rodríguez, and A. Barletta, "Linear disturbance growth induced by viscous dissipation in Darcy–Bénard convection with throughflow," Journal of Fluid Mechanics **974**, A15 (2023).
[10]D. A. Nield and A. Bejan, *Convection in Porous Media*, Vol. 3 (Springer, 2006).
[11]A. Delache, M. N. Ouarzazi, and M. Combarnous, "Spatio-temporal stability analysis of mixed convection flows in porous media heated from below: Comparison with experiments," International Journal of Heat and Mass Transfer **50**, 1485–1499 (2007).
[12]A. Barletta and L. S. d. B. Alves, "Absolute instability: A toy model and an application to the Rayleigh–Bénard problem with horizontal flow in porous media," International Journal of Heat and Mass Transfer **104**, 438–455 (2017).
[13]D. E. Ashpis and E. Reshotko, "The vibrating ribbon problem revisited," Journal of Fluid Mechanics **213**, 531–547 (1990).
[14]A. Tumin, "Receptivity of pipe Poiseuille flow," Journal of Fluid Mechanics **315**, 119–137 (1996).
[15]P. Huerre and M. Rossi, "Hydrodynamic instabilities in open flows: Hydrodynamics and nonlinear instabilities, edited by c. godrèche and p. manneville," (1998).
[16]M. Gaster, "On the generation of spatially growing waves in a boundary layer," Journal of Fluid Mechanics **22**, 433–441 (1965).
[17]A. Barletta, "Spatially developing modes: The Darcy–Bénard problem revisited," Physics **3**, 549–562 (2021).
[18]A. Barletta, "Time-evolving to space-evolving Rayleigh–Bénard instability of a horizontal porous medium flow," Physics of Fluids **33**, 124106 (2021).
[19]F. Dufour and M.-C. Neel, "Numerical study of instability in a horizontal porous channel with bottom heating and forced horizontal flow," Physics of Fluids **10**, 2198–2207 (1998).
[20]F. Dufour and M.-C. Néel, "Time-periodic convective patterns in a horizontal porous layer with through-flow," Quarterly of Applied Mathematics , 265–281 (2000).
[21]H. Bénard, "Les tourbillons cellulaires dans une nappe liquide.-méthodes optiques d'observation et d'enregistrement," Journal de Physique Théorique et Appliquée **10**, 254–266 (1901).
[22]L. Rayleigh, "On convection currents in a horizontal layer of fluid, when the higher temperature is on the under side," The London, Edinburgh, and Dublin Philosophical Magazine and Journal of Science **32**, 529–546 (1916).
[23]M. Combarnous and S. Bories, "Hydrothermal convection in saturated porous media," in *Advances in hydroscience*, Vol. 10 (Elsevier, 1975) pp. 231–307.
[24]J. B. Freund, "Proposed inflow/outflow boundary condition for direct computation of aerodynamic sound," AIAA journal **35**, 740–742 (1997).

[25]S. K. Richards, X. Zhang, X. Chen, and P. A. Nelson, "The evaluation of non-reflecting boundary conditions for duct acoustic computation," Journal of Sound and Vibration **270**, 539–557 (2004).